

SUPPORTING ONLINE MATERIAL

Methods

Stable isotopes

Stable oxygen ($\delta^{18}\text{O}$) and carbon ($\delta^{13}\text{C}$) isotopes along 36-m long IMAGES core MD97-2120 were analyzed on mono-specific samples of the benthic foraminifers *Cibicidoides wuellerstorfi*, *C. cicatricosus* and *C. kullenbergi* (>250 μm). In core sections lacking *Cibicidoides* spp., the isotope profiles were complemented by measurements on *Melonis barleeanum* and *Bulimina aculeata*. Isotope samples contained 1-7 specimens of *Cibicidoides* spp. and 2-10 specimens of *M. barleeanum* and were cleaned following standard laboratory protocols (S1). Isotope analyses were performed using a ThermoFinnigan MAT 252 mass spectrometer with automated Carbo Kiel III carbonate preparation device. Precision over the period of analysis was 0.02‰ and 0.01‰ for $\delta^{18}\text{O}$ and $\delta^{13}\text{C}$, respectively, as checked by routine runs of NBS19.

Inter-species $\delta^{18}\text{O}$ and $\delta^{13}\text{C}$ offsets were checked against *C. wuellerstorfi* values using paired analyses and adjusted if necessary. *C. kullenbergi*, *M. barleeanum* and *B. aculeata* $\delta^{18}\text{O}$ values were adjusted by -0.18‰, -0.15‰ and -0.7‰, respectively, based on constant offsets from *C. wuellerstorfi* values. $\delta^{13}\text{C}$ of *C. cicatricosus* and *B. aculeata* was adjusted by +0.3‰ and +0.4‰, respectively. The $\delta^{13}\text{C}$ values of *M. barleeanum* show a $\delta^{18}\text{O}$ -dependent offset from *C. wuellerstorfi* ($\delta^{13}\text{C}$ offset = $-0.7\delta^{18}\text{O}_{Mb} + 4.4$). The time-varying offset between both species likely reflects increased organic compound remineralization in pore waters that then are recorded by the endobenthic species, *M. barleeanum*. An empirical fit has been used to convert down core $\delta^{13}\text{C}$ values of *M. barleeanum* to equivalent values of *C. wuellerstorfi*.

Benthic $\delta^{18}\text{O}$ values, once adjusted to the *C. wuellerstorfi* scale of $\delta^{18}\text{O}$, were converted to $\delta^{18}\text{O}$ equilibrium values by adding 0.64‰ (S2). All isotope values are reported on the VPDB scale. Inter-specific benthic $\delta^{13}\text{C}$ correlation plots and converted benthic $\delta^{13}\text{C}$ and $\delta^{18}\text{O}$ data along core MD97-2120 are shown in Figures S1 and S2.

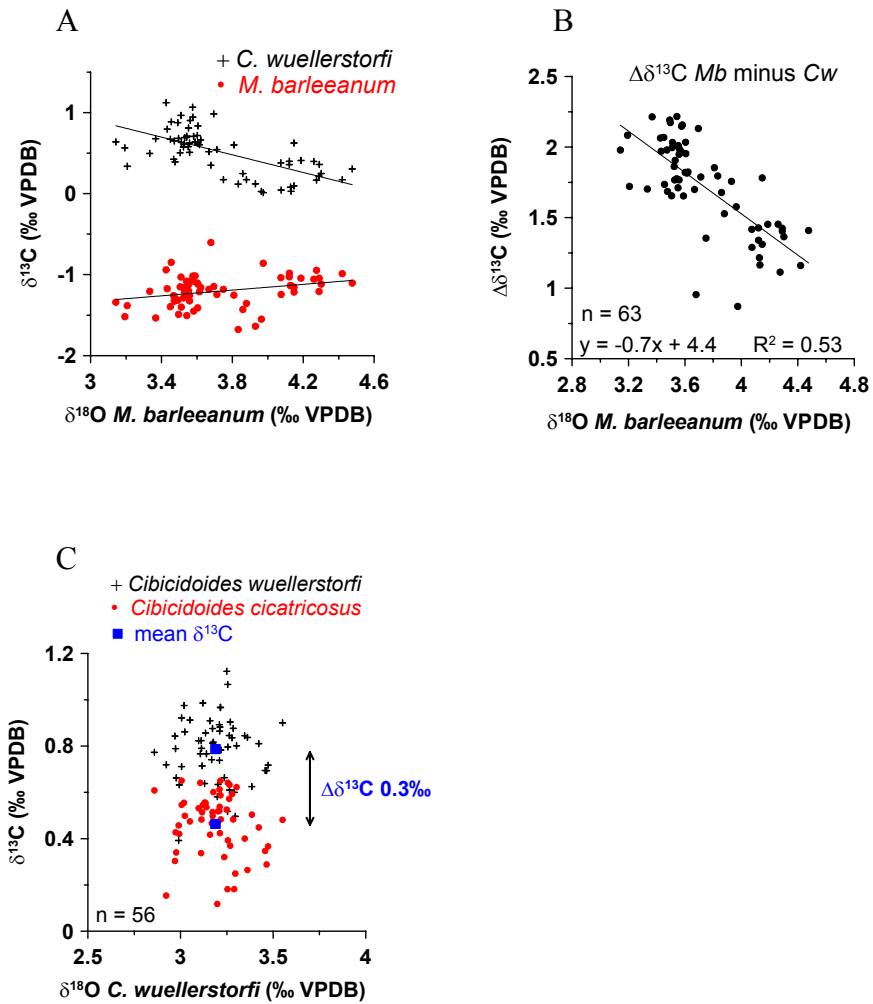


Fig. S1: **A** Regression plots of $\delta^{13}\text{C}$ for *M. barleeanum* (red dots) and *Cibicidoides wuellerstorfi* (black crosses) vs. $\delta^{18}\text{O}$ of *M. barleeanum*. The correlation shows a $\delta^{18}\text{O}$ -dependent $\delta^{13}\text{C}$ offset of *M. barleeanum* from $\delta^{13}\text{C}$ of *C. wuellerstorfi*. **B** Interspecific $\delta^{13}\text{C}$ offset between *M. barleeanum* and *C. wuellerstorfi* plotted vs. $\delta^{18}\text{O}$ of *M. barleeanum*. **C** $\delta^{13}\text{C}$ of *C. wuellerstorfi* (crosses) and *C. cicatricosus* (red dots) vs. $\delta^{18}\text{O}$ of *C. wuellerstorfi*; blue squares indicate mean $\delta^{13}\text{C}$ values for each species with an average interspecific offset of $\Delta\delta^{13}\text{C} = 0.3\text{‰}$.

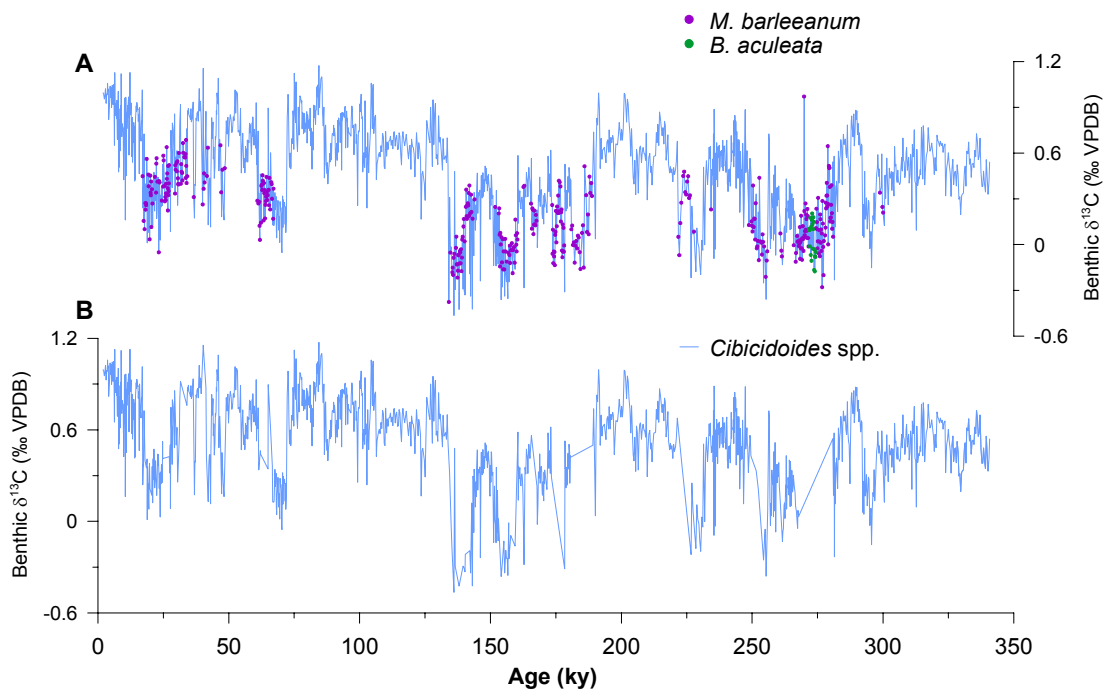


Fig. S2: Benthic $\delta^{13}\text{C}$ along core MD97-2120 highlighting different benthic species used for analysis. **(A)** Benthic $\delta^{13}\text{C}$ record combining values of all species (blue curve, converted to the *C. wuellerstorfi* scale as described above and shown in Figure S1). Different species are indicated by symbols (see Figure legend). **(B)** Benthic $\delta^{13}\text{C}$ record combining only $\delta^{13}\text{C}$ values of *Cibicidoides* spp. Low glacial values, abrupt increases at glacial terminations and millennial-scale $\delta^{13}\text{C}$ variability are seen in (B) i.e., they are robust features and not biased by the additional use of endobenthic foraminiferal species.

Age model

The age scale for core MD97-2120 was established previously (*S3*, *S4*) and is used in this study with a slight modification in the age range 29-35 ky. The age scale is based on 13 calibrated ^{14}C ages, the Kawakawa tephra and benthic $\delta^{18}\text{O}$ and $\text{SST}_{\text{Mg/Ca}}$ tuning to North Atlantic core MD95-2042 (*S5*) and the Vostok ice core deuterium record (*S6*) (on the orbitally tuned age scale of (*S7*)), respectively. In the following, we describe the age control in the interval 0-40 ky based on radiocarbon dating, as the age scale in this section deviates slightly from the previously published age scale of (*S3*). Details regarding age control in the older sections of core MD97-2120 can be found in the Supplementary Online Material accompanying the previous publication (*S4*).

Planktonic ^{14}C ages younger than 20 ky were calibrated to calendar ages using the marine INTCAL98 calibration curve integrated in the Calib4.3 program (*S8*, *S9*). A local ^{14}C reservoir age correction of 240 ± 40 yr (*S10*) was applied to these dates prior to calibration (resulting in a total reservoir correction of ~ 640 yr). In deviation from the previous age model of (*S3*), we calibrated the three ^{14}C dates between 26.6 and 32.3 ^{14}C ky using a new calibration data set (*S11*) that is tied to the Greenland GISP2 chronology of ref. (*S12*) and provides best available constraint in this age range. The glacial-age ^{14}C dates were reservoir-corrected by 1,970 yr, the reservoir age determined from paired Kawakawa ash and marine sediment radiocarbon dating east of New Zealand (*S10*).

Two ^{14}C dates (16.38, 16.67 ka, equivalent to 18.68, 19.01 cal. ka) were discarded that deviate considerably from the otherwise strongly linear age vs. core-depth correlation (Fig. S3). Both dates were generated from small carbonate samples causing concern regarding their reliability. Two age reversals occur in the sequence of AMS datings, one at 168-193 cm and one at 266-303 cm. In both cases we applied interpolated ages from the linear age vs. depth relation (Fig. S3).

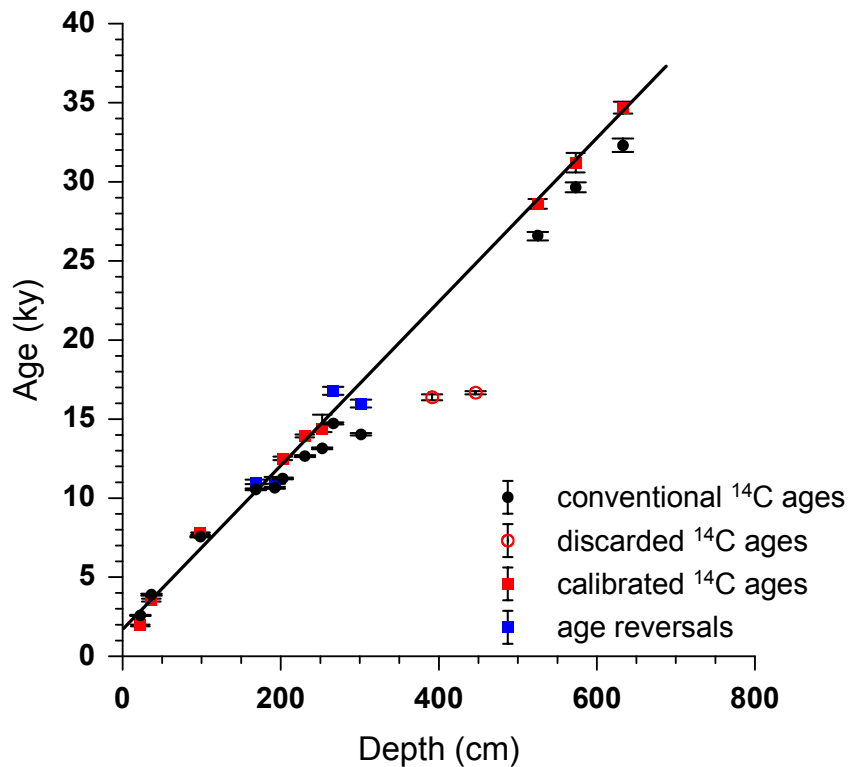


Fig. S3: ^{14}C AMS ages for core MD97-2120. Uncorrected radiocarbon ages (black dots) and calibrated ages (red squares) plotted against depth in core. Discarded dates are shown as open red circles. Blue squares are age reversals for which interpolated ages were computed applying the linear age vs. depth regression through all calibrated ages except for the two rejected ages ($y = 0.0518x + 1.6941$, $R^2 = 0.998$). The mean of two interpolated ages was then used for the age model of MD97-2120.

New absolute "SFCP" age scale of ref. (S13) for Greenland ice cores and MD95-2042

Shackleton *et al.* (S13) recently developed a new absolute age scale ("SFCP") for the Greenland ice cores (GISP2, GRIP) and North Atlantic core MD95-2042 that affects our age scale in two ways: 1) The ^{14}C -calendar age calibration of (S11) that we used to calibrate three ^{14}C ages between 26.6 and 32.3 ^{14}C ky (see above) is tied to the original GISP2 chronology of ref. (S12). 2) The interval 40-72 ky of our core has been tuned initially to the previously published age scale of MD95-2042 of (S5), which was likewise tied to the original GISP2 age scale of ref. (S12). The new SFCP age scale also impinges on the Vostok age scale in similar ways. Transferring the SFCP age scale to our core and the GISP2 and Vostok record therefore alters the absolute age scale, but leaves the comparisons

shown in Figs. 2, 3 and 4 of the main text intact as those changes affect age scales of both the ice core records and our benthic records, as well as that of the benthic record from Site 1089, in the same way. We thus chose to keep the original age scale for core MD97-2120 to allow comparison of our records with those from other cores whose age scales have not yet been modified with respect to the SFCP scale of (S13). We have, however, added an alternative age scale to our figures that shows the changes in age scale that arise from the new SFCP scale, including the ^{14}C -calendar age calibration curve of ref. (S11)) and benthic $\delta^{18}\text{O}$ correlation with MD95-2042 between 40-72 ky. As mentioned, the choice of age scale affects all records used in our study in the same way and therefore does not alter the core-to-core comparison or the inferences drawn from such comparison.

Downcore benthic $\delta^{13}\text{C}$ variability

Benthic $\delta^{13}\text{C}$ ($\delta^{13}\text{C}_b$) along core MD97-2120 is reduced during glacial periods of the past 340 ky. Abrupt positive departures from these low glacial levels occur in pace with Southern Hemisphere warm anomalies as documented in the SST record of the same core (S3) and Antarctic climate records (S6, S14). $\delta^{13}\text{C}_b$ is derived from $\delta^{13}\text{C}$ of total dissolved carbon ($\delta^{13}\text{C}_{\text{TCO}_2}$) in the ocean that is controlled by biological nutrient cycling and water mass chemical "aging" (S15). This makes foraminiferal $\delta^{13}\text{C}_b$ a valuable proxy to reconstruct past water mass variability. Overprints from organic-debris fluff layers at the sediment-water interface underlying high-productivity areas have been suggested to lower benthic $\delta^{13}\text{C}$ levels (S16). Sediment geochemistry on Chatham Rise indicates that marine biological productivity was increased during glacials (e.g., S17), but from paired $\delta^{13}\text{C}_b$ analyses of epibenthic and endobenthic species we do not find a measurable influence of productivity effects on the $\delta^{13}\text{C}$ composition of epibenthic *Cibicidoides* spp. in core MD97-2120 (Figs. S1, S2). Temperature-dependent $\delta^{13}\text{C}$ fractionation (S18) and source-water ("preformed") $\delta^{13}\text{C}_{\text{TCO}_2}$ changes can likewise be ruled out as drivers of the down-core $\delta^{13}\text{C}_b$ variability along our record. Air-sea fractionation tends to increase $\delta^{13}\text{C}_{\text{TCO}_2}$ values as ambient temperatures decrease, yet $\delta^{13}\text{C}_b$ maximizes along our record during Southern Hemisphere warming (Fig. 2) (S3, S6). Furthermore, the lack of coherency between $\delta^{13}\text{C}_b$

and planktonic $\delta^{13}\text{C}$ from our and other subantarctic core sites (e.g., core E11-2, 56°S (S19)) (Fig. S5) suggests that $\delta^{13}\text{C}_b$ in core MD97-2120 is not controlled by $\delta^{13}\text{C}$ changes at the AAIW source (S20).

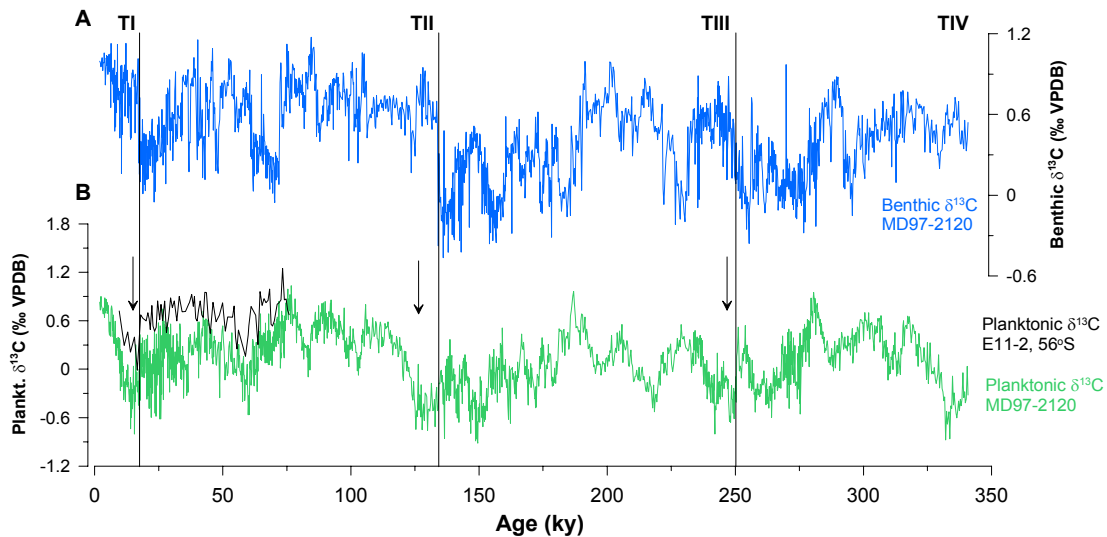


Fig. S4: Benthic (A) and planktonic (B) foraminiferal $\delta^{13}\text{C}$ records along core MD97-2120 (blue, green) and core E11-2 (black, Subantarctic Pacific 56°S (S19)). The structure of the planktonic (*Globigerina bulloides*) $\delta^{13}\text{C}$ record closely follows that of other subantarctic planktonic $\delta^{13}\text{C}$ records (e.g., of core E11-2, black curve in (B)), including the systematic minima during early deglaciations (arrows) described by Spero and Lea (S20). Lack of coherency between the benthic and planktonic records provides clear evidence that intermediate water $\delta^{13}\text{C}$ variability in core MD97-2120 is not controlled by (preformed) changes in the formation regions of Antarctic Intermediate Water (AAIW).

Similarity between subantarctic and tropical Pacific planktonic $\delta^{13}\text{C}$ patterns has been used as evidence for the transfer of $\delta^{13}\text{C}$ signals from high southern latitudes to the tropics, primarily through northward advection of AAIW (S20, S21). Marked differences between the planktonic and benthic $\delta^{13}\text{C}$ records from core MD97-2120 suggest that such $\delta^{13}\text{C}$ -signal transfer, if indeed operational, must have occurred outside the AAIW domain e.g., at shallower water depth of the thermocline and/or within the Subantarctic Mode Water (SAMW) layer. Such contention would be consistent with the recent notion (S22) that SAMW constitutes the main conduit for nutrient supply from the Southern Ocean to the tropical Pacific.

Supplementary Figure S5:

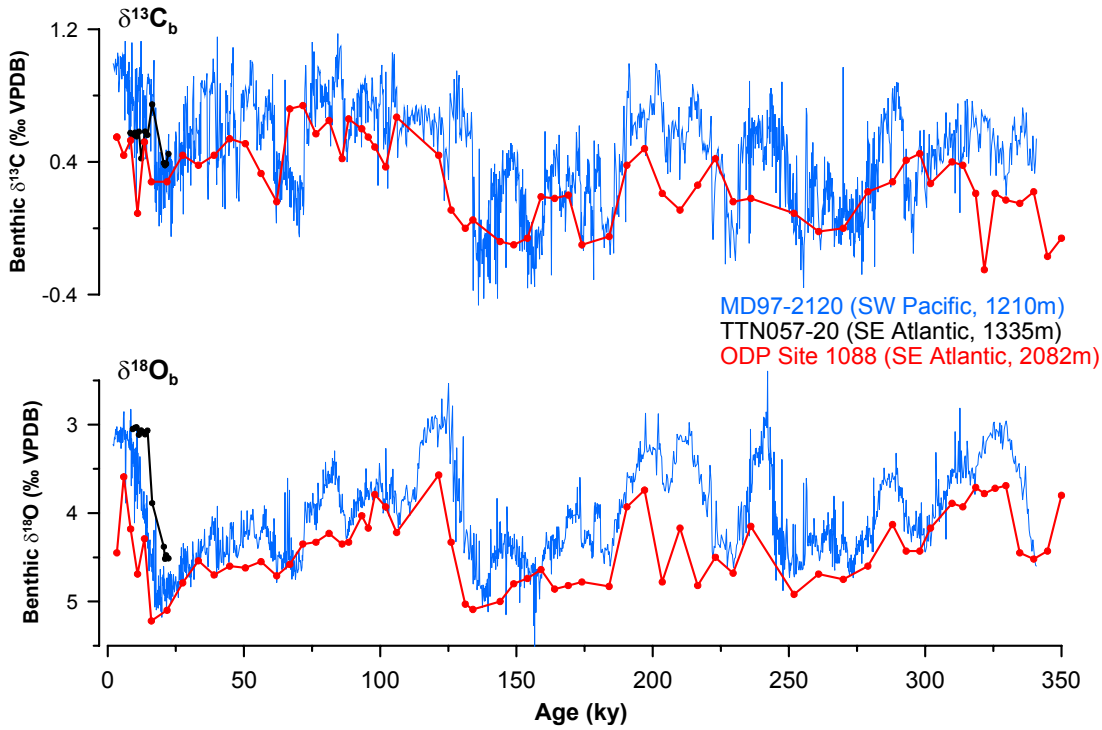


Fig. S5: Mid-depth $\delta^{13}\text{C}_b$ records from the SW Pacific (core MD97-2120, blue) and the SE Atlantic (core TN057-20, black (S21); ODP Site 1088, red (S23)). The benthic $\delta^{18}\text{O}$ records (bottom panel) are shown for stratigraphic reference. The $\delta^{13}\text{C}_b$ record from Site 1088 shows a similar pattern as the SW Pacific record over the past 340 ky and a similar amplitude at Termination II, keeping the lower temporal resolution of the record in mind. Late Holocene $\delta^{18}\text{O}_b$ at Site 1088 remains high, pointing to the possibility of disturbance of the uppermost section with the implication that $\delta^{13}\text{C}_b$ in this interval may not adequately reflect mid-depth ventilation changes. Likewise, we are not convinced that $\delta^{13}\text{C}_b$ in core TN057-20 covers the full glacial-interglacial transition during Termination I. However, we can not unambiguously rule out the possibility that the different $\delta^{13}\text{C}_b$ amplitudes during TI seen in the comparison reflect genuine differences in mid-depth ventilation between the SE Atlantic and SW Pacific.

Supplementary References:

- S1. R. Zahn *et al.*, *Paleoceanography* **12**, 696 (1997).
- S2. N. J. Shackleton, N. D. Opdyke, *Quat. Res.* **3**, 39 (1973).
- S3. K. Pahnke, R. Zahn, H. Elderfield, M. Schulz, *Science* **301**, 948 (2003).
- S4. Supporting Online Material for Pahnke *et al.* (2003):
<http://www.sciencemag.org/cgi/content/full/301/5635/948/DC1>
- S5. N. J. Shackleton, M. A. Hall, E. Vincent, *Paleoceanography* **15**, 565 (2000).
- S6. J. R. Petit *et al.*, *Nature* **399**, 429 (1999).
- S7. N. J. Shackleton, *Science* **289**, 1897 (2000).
- S8. M. Stuiver, P. J. Reimer, *Radiocarbon* **35**, 215 (1993).
- S9. M. Stuiver *et al.*, *Radiocarbon* **40**, 1041 (1998).
- S10. E. L. Sikes, C. R. Samson, T. P. Guilderson, W. R. Howard, *Nature* **405**, 555 (2000).
- S11. K. A. Hughen *et al.*, *Science* **303**, 202 (2004).
- S12. D. A. Meese *et al.*, *J. Geophys. Res.* **102**, 26411 (1997).
- S13. N. J. Shackleton, R. G. Fairbanks, T.-C. Chiu, F. Parrenin, *Quat. Sci. Rev.* **23**, 1513 (2004).
- S14. T. Blunier *et al.*, *Nature* **394**, 739 (1998).
- S15. P. M. Kroopnick, *Deep-Sea Res.* **32**, 57 (1985).
- S16. A. Mackensen, H. W. Hubberten, T. Bickert, G. Fischer, D. K. Fuetterer, *Paleoceanography* **8**, 587 (1993).
- S17. C. M. B. Lean, I. N. McCave, *Earth Planet. Sci. Lett.* **163**, 247 (1998).
- S18. W. S. Broecker, E. Maier-Reimer, *Global Biogeochem. Cycles* **6**, 315 (1992).
- S19. U. S. Ninnemann, C. D. Charles, *Paleoceanography* **12**, 560 (1997).
- S20. H. J. Spero, D. W. Lea, *Science* **296**, 522 (2002).
- S21. U. S. Ninnemann, C. D. Charles, *Earth Planet. Sci. Lett.* **201**, 383 (2002).
- S22. J. L. Sarmiento, N. Gruber, M. A. Brzezinski, J. P. Dunne, *Nature* **427**, 56 (2004).
- S23. D. A. Hodell, K. A. Venz, C. D. Charles, U. S. Ninnemann, *Geochem. Geophys. Geosyst.* **4**, 1004 (2003).